Angewandte Chemie
Eine Zeitschrift der Gesellschaft Deutscher Chemiker

Supporting Information

Computational Identification and Experimental Demonstration of High-Performance Methane Sorbents

K. Nath, A. Ahmed, D. J. Siegel, A. J. Matzger**

Supporting Information

Table of Contents

SUPPORTING INFORMATION

1. Computational details

Calculation of crystallographic properties of MOFs. The crystallographic properties of all MOFs were calculated using the Zeo++ code,[1–3] which employs Voronoi tessellation techniques to evaluate properties related to MOF porosity.[2,3] A nitrogen molecule with kinetic diameter of 3.72 Å was used as a probe to calculate the surface area per unit mass (gravimetric surface area: gsa) and per unit volume (volumetric surface area: vsa), the largest cavity diameter (lcd), and pore limiting diameter (pld) .

***Grand Canonical Monte Carlo (GCMC) calculations*.** The CH_4 capacities of MOFs were computed using GCMC[10–14] as implemented in the RASPA[15] code. CH_4 adsorption was calculated at 298K for pressures of 5, 65, and 80 bar. For selected MOFs, full isotherms were evaluated. CH_4 capacity at a given temperature and pressure was evaluated by averaging the number of CH_4 molecules in the simulation cell over multiple GCMC cycles. At each cycle, translation, insertion and deletion of CH_4 molecules were performed with equal probabilities. For CUS MOFs using the quantum-mechanically tuned MOMs potential,[9] and for MOFs without CUS, CH_4 isotherm data was collected from 3000 production cycles, preceded by 2,000 initialization cycles. For CUS MOFs where the UFF(MOF)/9-site(CH_4) potential was used,[7,8] electrostatic interactions between MOF and CH_4 molecules were accounted for using an Ewald summation;[15] charges on the MOF atoms were calculated using the 'charge equilibration'[16,17] (Qeq) method.[15] In this case, CH_4 adsorption isotherm data was collected from 6000 production cycles, preceded by 4,000 initialization cycles. All MOFs were treated as rigid frameworks during CH_4 uptake calculations.[4]

Computational screening. 11,185 'real' MOFs were screened from the CoRE[18] (2019) database using GCMC calculations. Among these MOFs, 7,351 contain CUS, and 3,834 are non-CUS MOFs. Screening results based on the MOMs (Michigan Open Metal Site)[9] potential for the CUS MOFs are presented in Figure 1 and in Tables S2 & S3. Figure 1 and Tables S4 & S5 present similar results for the non-CUS MOFs as calculated with the DREIDING(MOF)/TraPPE(CH_4)[5,6] interatomic potential. Subsequently, a sub-set of this data set was re-evaluated with an additional set of interatomic potentials: UFF(MOF)/TraPPE(CH_4)[4,5] for non-CUS MOFs and the UFF(MOF)/9-site(CH_4)[7,8] for CUS MOFs. This choice of potentials yielded superior agreement with the isotherms measured for the MOFs examined here (Table 1 & Figures S13-S14).

SUPPORTING INFORMATION

Table S1 shows 7 out of 9 screening studies predominantly used Universal Force Field (UFF) and TraPPE interatomic potential parameters to represent MOF and CH_4 molecules, respectively, without benchmarking. Only 2 studies by Bao et al. used UFF interatomic potential parameters for both MOF and CH_4 molecules, aging without any benchmarking. In contrast to previous studies, we used two separate sets of interatomic potential parameters for CUS and non-CUS MOFs to identify the high-capacity MOFs that were previously overlooked due to the limitation of the general interatomic potentials.

Table S1. Summary of recent high-throughput calculations of CH_4 storage in MOFs.

Source	Database	No. MOFs screened	Interatomic potential parameters (MOF/CH_4)	Storage condition
Chung et al. (2014)	Real MOFs: CoRE 2014	5,309	UFF / TraPPE	Usable: (298 K, 65 bar) → (298 K, 5.8 bar) Total: 0.01, 5.8, and 65 bar at 298 K
Simon et al. (2015)			UFF / TraPPE	Usable: (77 & 298 K, 100 bar) → (77 & 298 K, 1 bar)
Simon et al. (2015)	Northwestern (hypothetical)	137,953	UFF / TraPPE	Usable: (77 & 298 K, 100 bar) → (77 & 298 K, 1 bar)
Fernandez et al. (2013)			UFF / TraPPE	Total: 1, 35, and 100 bar at 298 K
Wilmer et al. (2012)			UFF / TraPPE	Total: 35 bar at 298 K
Bao et al. (2015)	In-silico deliverable (hypothetical)	2,816	UFF / UFF	Usable: (298 K, 65 bar) → (298 K, 5.8 bar)
Bao et al. (2015)	In-silico surface (hypothetical)	8,885	UFF / UFF	Usable: (298 K, 35 or 65 bar) → (298 K, 5.8 bar)
Colón et al. (2017)	ToBaCCo (hypothetical)	13,512	UFF / TraPPE	Total: 6, 65, & 100 bar at 298 K
Gomez-Gualdron et al. (2014)	Zr-MOFs (hypothetical)	204	UFF / TraPPE	Usable: (298 K, 65 bar) → (298 K, 5.8 bar)

Table S2. Usable capacities (pressure swing between 65 and 5 bar) and crystallographic properties of the top 50 CUS MOFs. Screening was conducted based on the MOMs[9] interatomic potential.

Name	Source	Density (g/cm^3)	Gravimetric surface area (m^2/g)	Volumetric surface area (m^2/cm^3)	Void fraction	Pore volume (cm^3/g)	Largest cavity diameter (Å)	Pore limiting diameter (Å)	Usable gravimetric capacity (g/g)	Usable volumetric capacity (cm^3 STP/cm^3)
HKUST-1									**0.154**	**190**
NAFSOF_clean	CoRE (2019)	0.44	5220	2285	0.82	1.9	10.4	8.3	0.358	219
RICBEM_clean	CoRE (2019)	0.40	5705	2277	0.82	2.1	11.4	8.6	0.385	215
RAYMIP_clean	CoRE (2019)	0.50	4196	2110	0.81	1.6	13.5	9.8	0.305	214
MIXZOK_clean	CoRE (2019)	0.45	4658	2109	0.81	1.8	13.2	9.8	0.339	214
BICPUA_clean	CoRE (2019)	0.54	3872	2106	0.82	1.5	13.8	9.9	0.281	214
HAVZIP_clean	CoRE (2019)	0.42	4690	1955	0.82	2.0	13.0	9.6	0.366	213
ZAHLEC_clean	CoRE (2019)	0.50	5357	2701	0.81	1.6	10.7	8.4	0.302	213
ic800131r-file003_clean	CoRE (2019)	0.42	4750	1983	0.82	2.0	12.9	9.6	0.364	212
IDEYOF_clean	CoRE (2019)	0.43	5779	2478	0.81	1.9	10.0	6.2	0.355	212
RAYMOV_clean	CoRE (2019)	0.42	4982	2113	0.81	1.9	13.9	9.7	0.357	211
MAHCEG_clean	CoRE (2019)	0.53	4046	2149	0.81	1.5	18.5	8.0	0.285	211
BEWCUD_clean	CoRE (2019)	0.48	4457	2124	0.82	1.7	11.4	9.6	0.317	211
FISGOF_clean	CoRE (2019)	0.43	4624	2007	0.84	1.9	15.8	8.6	0.348	211
XOVPUU_clean	CoRE (2019)	0.40	4969	2012	0.84	2.1	11.5	9.8	0.370	209
TOVJAR_clean	CoRE (2019)	0.52	4005	2068	0.81	1.6	12.4	8.5	0.289	208
JOGSAA_clean	CoRE (2019)	0.42	4728	1990	0.82	2.0	13.0	9.4	0.354	208
BAZFUF_clean	CoRE (2019)	0.34	5368	1825	0.86	2.5	20.2	8.6	0.437	208
XEBHOC_clean	CoRE (2019)	0.47	4693	2182	0.81	1.7	12.1	9.9	0.320	208
TOVJIZ_clean	CoRE (2019)	0.45	4504	2032	0.80	1.8	12.7	8.3	0.329	207
BAZFUF01_clean	CoRE (2019)	0.34	5354	1831	0.86	2.5	20.1	8.5	0.432	207
XAWVUN_clean	CoRE (2019)	0.46	4721	2192	0.81	1.7	10.8	9.2	0.317	206
ZIJSAO_clean	CoRE (2019)	0.47	4735	2204	0.81	1.7	20.3	7.5	0.316	206
POHWIU_clean	CoRE (2019)	0.46	4230	1949	0.81	1.8	15.9	10.4	0.319	206
LURRIA_clean	CoRE (2019)	0.41	4611	1874	0.83	2.1	22.4	9.7	0.362	206
VOLRAQ01_clean	CoRE (2019)	0.56	3315	1861	0.84	1.5	16.9	11.2	0.262	205
ANUGIA_clean	CoRE (2019)	0.57	4061	2306	0.79	1.4	13.9	6.8	0.258	205
SETTAO_clean	CoRE (2019)	0.53	3851	2057	0.79	1.5	13.9	10.0	0.274	205
ANUGOG_clean	CoRE (2019)	0.58	4228	2472	0.79	1.4	11.4	7.1	0.249	204
XAFFER_clean	CoRE (2019)	0.36	5153	1854	0.85	2.4	14.2	13.3	0.405	203
FATQID_clean	CoRE (2019)	0.61	3634	2205	0.80	1.3	11.5	8.6	0.240	203
TOVJEV_clean	CoRE (2019)	0.40	4737	1893	0.84	2.1	13.7	10.4	0.364	203
XAFFAN_clean	CoRE (2019)	0.37	5192	1896	0.85	2.3	14.9	13.2	0.398	203
ENIHUG01_clean	CoRE (2019)	0.59	3971	2323	0.77	1.3	13.8	6.8	0.248	203
WAVQOB_clean	CoRE (2019)	0.66	2985	1981	0.77	1.2	10.3	8.2	0.219	203
EFAYIU_clean	CoRE (2019)	0.43	5192	2251	0.82	1.9	11.6	8.6	0.335	203
CAVPUM_manual	CoRE (2019)	0.41	4768	1943	0.82	2.0	20.4	7.8	0.356	202
VAGMAT_clean	CoRE (2019)	0.36	5141	1875	0.86	2.4	14.9	13.3	0.397	202
NAYZOE_clean	CoRE (2019)	0.50	4615	2302	0.81	1.6	15.8	6.5	0.290	202
ATEYED_clean	CoRE (2019)	0.47	7061	3303	0.78	1.7	7.5	6.2	0.309	202
MINCUJ_clean	CoRE (2019)	0.69	2920	2024	0.76	1.1	12.0	7.6	0.208	202
VAGMEX_clean	CoRE (2019)	0.35	5189	1828	0.86	2.5	15.3	14.5	0.410	202
ANUGEW_clean	CoRE (2019)	0.44	4709	2088	0.83	1.9	14.4	10.2	0.325	201
ACUFEK_clean	CoRE (2019)	0.56	3942	2205	0.79	1.4	15.6	9.0	0.258	201
ENIHUG_clean	CoRE (2019)	0.58	4025	2341	0.79	1.4	13.8	6.8	0.247	201
ASIVAB_clean	CoRE (2019)	0.54	4325	2328	0.80	1.5	12.3	7.3	0.267	201
DICKEH_clean	CoRE (2019)	0.52	4507	2355	0.80	1.5	12.8	7.4	0.274	200
YIPDOR_clean	CoRE (2019)	0.45	5445	2441	0.80	1.8	10.3	7.5	0.318	199
XAFFOB_clean	CoRE (2019)	0.37	5119	1879	0.85	2.3	14.8	13.2	0.389	199
RUVKAV_clean	CoRE (2019)	0.60	3706	2230	0.78	1.3	12.0	7.2	0.236	199
VANNIK_clean	CoRE (2019)	0.49	3703	1808	0.85	1.7	12.1	10.7	0.291	199

Table S3. Usable capacities (pressure swing between 80 and 5 bar) and crystallographic properties of the top 50 CUS MOFs. Screening was conducted based on the MOMs[9] interatomic potential.

Name	Source	Density (g/cm^3)	Gravimetric surface area (m^2/g)	Volumetric surface area (m^2/cm^3)	Void fraction	Pore volume (cm^3/g)	Largest cavity diameter (Å)	Pore limiting diameter (Å)	Usable gravimetric capacity (g/g)	Usable volumetric capacity (cm^3 STP/cm^3)
HKUST-1									**0.162**	**200**
NAFSOF_clean	CoRE (2019)	0.44	5220	2285	0.82	1.9	10.4	8.3	0.380	232
RICBEM_clean	CoRE (2019)	0.40	5705	2277	0.82	2.1	11.4	8.6	0.414	231
BAZFUF_clean	CoRE (2019)	0.34	5368	1825	0.86	2.5	20.2	8.6	0.482	229
BAZFUF01_clean	CoRE (2019)	0.34	5354	1831	0.86	2.5	20.1	8.5	0.477	228
HAVZIP_clean	CoRE (2019)	0.42	4690	1955	0.82	2.0	13.0	9.6	0.391	228
BICPUA_clean	CoRE (2019)	0.54	3872	2106	0.82	1.5	13.8	9.9	0.300	228
FISGOF_clean	CoRE (2019)	0.43	4624	2007	0.84	1.9	15.8	8.6	0.375	227
RAYMOV_clean	CoRE (2019)	0.42	4982	2113	0.81	1.9	13.9	9.7	0.383	227
MIXZOK_clean	CoRE (2019)	0.45	4658	2109	0.81	1.8	13.2	9.8	0.359	227
ic800131r-file003_clean	CoRE (2019)	0.42	4750	1983	0.82	2.0	12.9	9.6	0.389	227
IDEYOF_clean	CoRE (2019)	0.43	5779	2478	0.81	1.9	10.0	6.2	0.378	226
XOVPUU_clean	CoRE (2019)	0.40	4969	2012	0.84	2.1	11.5	9.8	0.400	226
VOLRAQ01_clean	CoRE (2019)	0.56	3315	1861	0.84	1.5	16.9	11.2	0.288	226
RAYMIP_clean	CoRE (2019)	0.50	4196	2110	0.81	1.6	13.5	9.8	0.322	226
BEWCUD_clean	CoRE (2019)	0.48	4457	2124	0.82	1.7	11.4	9.6	0.338	225
ZAHLEC_clean	CoRE (2019)	0.50	5357	2701	0.81	1.6	10.7	8.4	0.319	225
JOGSAA_clean	CoRE (2019)	0.42	4728	1990	0.82	2.0	13.0	9.4	0.382	225
MAHCEG_clean	CoRE (2019)	0.53	4046	2149	0.81	1.5	18.5	8.0	0.302	224
TOVJAR_clean	CoRE (2019)	0.52	4005	2068	0.81	1.6	12.4	8.5	0.310	224
LURRIA_clean	CoRE (2019)	0.41	4611	1874	0.83	2.1	22.4	9.7	0.392	223
TOVJEV_clean	CoRE (2019)	0.40	4737	1893	0.84	2.1	13.7	10.4	0.397	221
XEBHOC_clean	CoRE (2019)	0.47	4693	2182	0.81	1.7	12.1	9.9	0.341	221
POHWIU_clean	CoRE (2019)	0.46	4230	1949	0.81	1.8	15.9	10.4	0.343	221
TOVJIZ_clean	CoRE (2019)	0.45	4504	2032	0.80	1.8	12.7	8.3	0.350	221
XAFFER_clean	CoRE (2019)	0.36	5153	1854	0.85	2.4	14.2	13.3	0.439	221
VAGMAT_clean	CoRE (2019)	0.36	5141	1875	0.86	2.4	14.9	13.3	0.433	220
XAWVUN_clean	CoRE (2019)	0.46	4721	2192	0.81	1.7	10.8	9.2	0.340	220
XAFFAN_clean	CoRE (2019)	0.37	5192	1896	0.85	2.3	14.9	13.2	0.432	220
ZIJSAO_clean	CoRE (2019)	0.47	4735	2204	0.81	1.7	20.3	7.5	0.338	220
VANNIK_clean	CoRE (2019)	0.49	3703	1808	0.85	1.7	12.1	10.7	0.322	220
ANUGEW_clean	CoRE (2019)	0.44	4709	2088	0.83	1.9	14.4	10.2	0.354	219
VAGMEX_clean	CoRE (2019)	0.35	5189	1828	0.86	2.5	15.3	14.5	0.446	219
FIFGEI_clean	CoRE (2019)	0.41	4211	1738	0.86	2.1	16.2	14.7	0.380	219
CAVPUM_manual	CoRE (2019)	0.41	4768	1943	0.82	2.0	20.4	7.8	0.385	219
SETTAO_clean	CoRE (2019)	0.53	3851	2057	0.79	1.5	13.9	10.0	0.292	218
EFAYIU_clean	CoRE (2019)	0.43	5192	2251	0.82	1.9	11.6	8.6	0.359	217
ANUGIA_clean	CoRE (2019)	0.57	4061	2306	0.79	1.4	13.9	6.8	0.273	217
XAFFOB_clean	CoRE (2019)	0.37	5119	1879	0.85	2.3	14.8	13.2	0.423	217
FATQID_clean	CoRE (2019)	0.61	3634	2205	0.80	1.3	11.5	8.6	0.256	217
XAFFIV_clean	CoRE (2019)	0.36	5300	1899	0.85	2.4	14.2	13.2	0.431	216
ANUGOG_clean	CoRE (2019)	0.58	4228	2472	0.79	1.4	11.4	7.1	0.263	215
NAYZOE_clean	CoRE (2019)	0.50	4615	2302	0.81	1.6	15.8	6.5	0.309	215
DICKEH_clean	CoRE (2019)	0.52	4507	2355	0.80	1.5	12.8	7.4	0.294	214
XAHPED_clean	CoRE (2019)	0.37	5199	1947	0.84	2.2	12.4	10.9	0.409	214
ASIVAB_clean	CoRE (2019)	0.54	4325	2328	0.80	1.5	12.3	7.3	0.284	214
WAVQOB_clean	CoRE (2019)	0.66	2985	1981	0.77	1.2	10.3	8.2	0.230	214
MINCUJ_clean	CoRE (2019)	0.69	2920	2024	0.76	1.1	12.0	7.6	0.221	213
UDANIY_clean	CoRE (2019)	0.42	4181	1745	0.85	2.0	23.9	23.5	0.366	213
ATEYED_clean	CoRE (2019)	0.47	7061	3303	0.78	1.7	7.5	6.2	0.325	213
cg500175k_si_001_auto	CoRE (2019)	0.52	3653	1882	0.82	1.6	20.4	9.9	0.295	213

Table S4. Usable capacities (pressure swing between 65 and 5 bar) and crystallographic properties of 50 promising non-CUS MOFs. Screening was conducted based on the DREIDING(MOF)/TraPPE(CH_4)[5,6] interatomic potential.

Name	Source	Density (g/cm^3)	Gravimetric surface area (m^2/g)	Volumetric surface area (m^2/cm^3)	Void fraction	Pore volume (cm^3/g)	Largest cavity diameter (Å)	Pore limiting diameter (Å)	Usable gravimetric capacity (g/g)	Usable volumetric capacity (cm^3 STP/cm^3)
HKUST-1									**0.154**	**190**
VEBHUG_SL	CoRE(2019)	0.51	3751	1917	0.85	1.7	17.3	9.8	0.271	194
FUYCIN_clean	CoRE(2019)	0.44	4293	1877	0.83	1.9	11.4	11.1	0.314	192
ja074366osi20070816_031204_clean	CoRE(2019)	0.60	3703	2203	0.81	1.4	15.0	8.0	0.225	187
PEVQOY_clean_h	CoRE(2019)	0.61	3637	2232	0.81	1.3	14.8	7.9	0.215	184
XIYYEL_clean	CoRE(2019)	0.72	3203	2313	0.79	1.1	8.5	8.2	0.185	186
VUSKEA_clean	CoRE(2019)	0.59	3687	2193	0.80	1.3	15.0	8.0	0.223	185
VUSKAW_clean	CoRE(2019)	0.59	3708	2205	0.80	1.3	15.0	8.0	0.223	185
cg500192d_si_003_clean	CoRE(2019)	0.55	3732	2069	0.79	1.4	11.2	9.5	0.240	186
EDUSIF_clean	CoRE(2019)	0.59	3751	2226	0.81	1.4	15.1	7.9	0.222	184
LAWGOG_clean	CoRE(2019)	0.59	3785	2231	0.80	1.4	15.1	7.9	0.220	181
LAWGEW_clean	CoRE(2019)	0.59	3769	2230	0.80	1.4	15.1	7.9	0.220	182
COXHON_clean	CoRE(2019)	0.66	3486	2298	0.80	1.2	8.8	8.5	0.197	182
LAWGIA_clean	CoRE(2019)	0.59	3776	2230	0.80	1.4	15.1	7.9	0.222	183
LAWFOF_clean	CoRE(2019)	0.59	3788	2233	0.81	1.4	15.1	8.0	0.220	181
HIFTOG01_clean	CoRE(2019)	0.58	3799	2219	0.80	1.4	15.1	7.9	0.222	181
LAWGUM_clean	CoRE(2019)	0.59	3790	2232	0.80	1.4	15.1	7.9	0.220	181
LAWFUL_clean	CoRE(2019)	0.59	3779	2229	0.81	1.4	15.1	8.0	0.219	180
LAWGAS_clean	CoRE(2019)	0.59	3787	2234	0.81	1.4	15.1	7.9	0.219	181
MEJMOE_clean	CoRE(2019)	0.62	3622	2232	0.81	1.3	13.4	7.2	0.207	178
NEYVEU_clean	CoRE(2019)	0.51	3905	2008	0.80	1.5	20.2	6.4	0.249	179
ja5b00365_si_002_clean	CoRE(2019)	0.45	4503	2038	0.83	1.8	21.8	7.6	0.282	178
ERIRIG_auto	CoRE(2019)	0.43	4770	2036	0.83	1.9	11.7	9.6	0.294	175
ic2017598_si_001_clean_h	CoRE(2019)	0.61	3715	2263	0.80	1.3	14.9	7.9	0.210	178
ICAQIO_clean	CoRE(2019)	0.40	4746	1915	0.83	2.0	20.4	8.0	0.312	176
PEVQIS_clean_h	CoRE(2019)	0.61	3681	2230	0.81	1.3	14.9	7.8	0.211	178
ICAQOU_clean	CoRE(2019)	0.41	4636	1916	0.82	2.0	20.3	7.9	0.303	175
VAZTOG_clean	CoRE(2019)	0.59	3787	2234	0.80	1.4	15.1	7.9	0.213	175
ICAROV_clean	CoRE(2019)	0.41	4744	1928	0.82	2.0	20.3	7.9	0.306	174
VAZTUM_clean	CoRE(2019)	0.59	3797	2247	0.81	1.4	15.1	7.9	0.215	178
KULMEK_clean	CoRE(2019)	0.66	3438	2269	0.75	1.1	13.2	7.5	0.191	176
PEDRIA_clean	CoRE(2019)	0.59	3806	2245	0.81	1.4	15.1	7.9	0.210	173
KINSEH_clean	CoRE(2019)	0.63	2959	1878	0.75	1.2	12.8	11.5	0.202	179
HAFTOZ_clean	CoRE(2019)	0.55	3683	2040	0.78	1.4	15.4	7.5	0.224	173
ja4015666_si_002_clean	CoRE(2019)	0.71	3127	2225	0.76	1.1	10.1	9.1	0.177	176
ja4015666_si_005_clean	CoRE(2019)	0.72	3075	2224	0.75	1.0	10.1	9.0	0.175	177
IYOWID_manual	CoRE(2019)	0.41	4764	1930	0.82	2.0	20.5	7.7	0.298	169
EDUVOO_clean	CoRE(2019)	0.37	4790	1788	0.86	2.3	20.9	10.6	0.317	166
FEFDEB_manual	CoRE(2019)	0.54	3959	2135	0.77	1.4	13.1	11.6	0.226	170
ja4015666_si_003_clean	CoRE(2019)	0.72	3143	2257	0.75	1.0	10.1	9.0	0.175	175
NEXVET_clean	CoRE(2019)	0.57	3880	2221	0.81	1.4	15.1	7.9	0.213	170
acs.jpcc.6b08594_Zn2Cd6MOF5_opt_clean	CoRE(2019)	0.63	3422	2151	0.81	1.3	14.7	8.1	0.189	166
LIRFIB_clean	CoRE(2019)	0.55	4061	2253	0.80	1.4	9.2	8.8	0.213	165
COXHIH_clean	CoRE(2019)	0.71	3273	2311	0.79	1.1	8.6	8.2	0.168	166
CAVPEW_manual	CoRE(2019)	0.40	4794	1931	0.82	2.0	20.3	7.8	0.293	165
QAMLEY_clean	CoRE(2019)	0.70	3269	2278	0.76	1.1	11.1	6.1	0.177	172
COXHED_clean	CoRE(2019)	0.69	3357	2309	0.80	1.2	8.7	8.4	0.171	164
ja5109535_si_002_clean	CoRE(2019)	0.65	3380	2199	0.77	1.2	17.5	7.7	0.188	171
GURPUF_clean	CoRE(2019)	0.70	3384	2357	0.79	1.1	9.5	8.4	0.170	165
CAVPIA_manual	CoRE(2019)	0.42	4733	1970	0.81	2.0	19.9	7.8	0.286	166
ic101935f_si_002_auto	CoRE(2019)	0.41	5095	2079	0.85	2.1	13.5	8.8	0.286	163

SUPPORTING INFORMATION

Table S5. Usable capacities (pressure swing between 80 and 5 bar) and crystallographic properties of 50 promising non-CUS MOFs. Screening was conducted based on the DREIDING(MOF)/TraPPE(CH_4)[5,6] interatomic potential.

Name	Source	Density (g/cm^3)	Gravimetric surface area (m^2/g)	Volumetric surface area (m^2/cm^3)	Void fraction	Pore volume (cm^3/g)	Largest cavity diameter (Å)	Pore limiting diameter (Å)	Usable gravimetric capacity (g/g)	Usable volumetric capacity (cm^3 STP/cm^3)
HKUST-1									**0.162**	**200**
VEBHUG_SL	CoRE(2019)	0.51	3751	1917	0.85	1.7	17.3	9.8	0.298	213
FUYCIN_clean	CoRE(2019)	0.44	4293	1877	0.83	1.9	11.4	11.1	0.344	210
ja074366osi20070816_031204_clean	CoRE(2019)	0.60	3703	2203	0.81	1.4	15.0	8.0	0.246	204
XIYYEL_clean	CoRE(2019)	0.72	3203	2313	0.79	1.1	8.5	8.2	0.200	202
cg500192d_si_003_clean	CoRE(2019)	0.55	3732	2069	0.79	1.4	11.2	9.5	0.259	200
VUSKAW_clean	CoRE(2019)	0.59	3708	2205	0.80	1.3	15.0	8.0	0.241	200
VUSKEA_clean	CoRE(2019)	0.59	3687	2193	0.80	1.3	15.0	8.0	0.243	202
PEVQOY_clean_h	CoRE(2019)	0.61	3637	2232	0.81	1.3	14.8	7.9	0.236	202
EDUSIF_clean	CoRE(2019)	0.59	3751	2226	0.81	1.4	15.1	7.9	0.241	200
LAWGIA_clean	CoRE(2019)	0.59	3776	2230	0.80	1.4	15.1	7.9	0.240	198
LAWGEW_clean	CoRE(2019)	0.59	3769	2230	0.80	1.4	15.1	7.9	0.241	199
COXHON_clean	CoRE(2019)	0.66	3486	2298	0.80	1.2	8.8	8.5	0.216	198
LAWGUM_clean	CoRE(2019)	0.59	3790	2232	0.80	1.4	15.1	7.9	0.240	197
LAWGOG_clean	CoRE(2019)	0.59	3785	2231	0.80	1.4	15.1	7.9	0.242	199
LAWFOF_clean	CoRE(2019)	0.59	3788	2233	0.81	1.4	15.1	8.0	0.240	198
LAWGAS_clean	CoRE(2019)	0.59	3787	2234	0.81	1.4	15.1	7.9	0.238	196
HIFTOG01_clean	CoRE(2019)	0.58	3799	2219	0.80	1.4	15.1	7.9	0.242	197
LAWFUL_clean	CoRE(2019)	0.59	3779	2229	0.81	1.4	15.1	8.0	0.239	197
KINSEH_clean	CoRE(2019)	0.63	2959	1878	0.75	1.2	12.8	11.5	0.214	189
NEYVEU_clean	CoRE(2019)	0.51	3905	2008	0.80	1.5	20.2	6.4	0.271	195
ic2017598_si_001_clean_h	CoRE(2019)	0.61	3715	2263	0.80	1.3	14.9	7.9	0.228	194
PEVQIS_clean_h	CoRE(2019)	0.61	3681	2230	0.81	1.3	14.9	7.8	0.228	193
ja5b00365_si_002_clean	CoRE(2019)	0.45	4503	2038	0.83	1.8	21.8	7.6	0.308	194
MEJMOE_clean	CoRE(2019)	0.62	3622	2232	0.81	1.3	13.4	7.2	0.227	196
VAZTUM_clean	CoRE(2019)	0.59	3797	2247	0.81	1.4	15.1	7.9	0.231	191
ja4015666_si_005_clean	CoRE(2019)	0.72	3075	2224	0.75	1.0	10.1	9.0	0.186	188
ja4015666_si_002_clean	CoRE(2019)	0.71	3127	2225	0.76	1.1	10.1	9.1	0.190	189
KULMEK_clean	CoRE(2019)	0.66	3438	2269	0.75	1.1	13.2	7.5	0.206	190
ICAQIO_clean	CoRE(2019)	0.40	4746	1915	0.83	2.0	20.4	8.0	0.344	194
ERIRIG_auto	CoRE(2019)	0.43	4770	2036	0.83	1.9	11.7	9.6	0.326	194
ICAQOU_clean	CoRE(2019)	0.41	4636	1916	0.82	2.0	20.3	7.9	0.334	193
ja4015666_si_003_clean	CoRE(2019)	0.72	3143	2257	0.75	1.0	10.1	9.0	0.186	186
VAZTOG_clean	CoRE(2019)	0.59	3787	2234	0.80	1.4	15.1	7.9	0.233	192
ICAROV_clean	CoRE(2019)	0.41	4744	1928	0.82	2.0	20.3	7.9	0.337	192
HAFTOZ_clean	CoRE(2019)	0.55	3683	2040	0.78	1.4	15.4	7.5	0.244	189
PEDRIA_clean	CoRE(2019)	0.59	3806	2245	0.81	1.4	15.1	7.9	0.231	190
QAMLEY_clean	CoRE(2019)	0.70	3269	2278	0.76	1.1	11.1	6.1	0.188	183
ic502725y_si_004_clean	CoRE(2019)	1.57	1304	2049	0.64	0.4	9.6	4.4	0.082	180
ja5109535_si_002_clean	CoRE(2019)	0.65	3380	2199	0.77	1.2	17.5	7.7	0.201	182
NEXVET_clean	CoRE(2019)	0.57	3880	2221	0.81	1.4	15.1	7.9	0.232	186
FEFDEB_manual	CoRE(2019)	0.54	3959	2135	0.77	1.4	13.1	11.6	0.247	186
WECBEN_clean	CoRE(2019)	0.99	3144	3119	0.70	0.7	6.5	4.3	0.128	178
ABETIN_clean	CoRE(2019)	0.60	3811	2276	0.73	1.2	9.5	7.8	0.215	180
IYOWID_manual	CoRE(2019)	0.41	4764	1930	0.82	2.0	20.5	7.7	0.331	187
WUTBEU_clean	CoRE(2019)	0.75	2277	1719	0.75	1.0	12.7	12.5	0.170	180
KEDJAG04_clean	CoRE(2019)	1.07	2815	3013	0.69	0.6	5.6	4.4	0.116	174
KEDJAG14_clean	CoRE(2019)	1.06	2872	3042	0.69	0.7	5.6	4.5	0.118	175
KEDJAG10_clean	CoRE(2019)	1.06	2853	3032	0.69	0.7	5.6	4.4	0.118	176
KEDJAG16_clean	CoRE(2019)	1.06	2877	3044	0.69	0.7	5.6	4.5	0.118	175
KEDJAG18_clean	CoRE(2019)	1.05	2902	3061	0.70	0.7	5.7	4.5	0.118	173

2. Materials

Terephthalic acid (98%), 4,4'-bipyridine (98%) and 1,3,5-tris(4-carboxyphenyl)benzene (98%) were purchased from Sigma-Aldrich and used as received. 1,3,5-Benzenetricarboxylic acid (98%), 2,5-dibromopyrimidine (98%), dimethyl 5-(4,4,5,5-tetramethyl-1,3,2-dioxaborolan-2-yl)isophthalate, copper(II) nitrate hemi(pentahydrate) (98%) and zinc(II) nitrate hexahydrate (98%, ACS grade) were purchased from Fisher Scientific. Zinc(II) nitrate hexahydrate (98%, ACS grade) was partially dehydrated at room temperature under dynamic evacuation (∽16h, <0.03Torr) to yield zinc(II) nitrate tetrahydrate. Organic linkers **H_4L1**[19] and **H_4L2**[20] were prepared according to reported literature procedure with slight modifications. N,N-Diethylformamide (DEF) (99%) was purchased from Acros Organics and was purified by storage on activated charcoal for ∽1 week and then passed through silica column gel to remove impurities and stored over 4Å molecular sieves. N,N-Dimethyl formamide (DMF, ACS grade), dichloromethane (DCM, ACS grade), n-hexane (ACS grade) and anhydrous methanol (98%, ACS grade) were purchased from Fisher Scientific and stored over activated 3Å molecular sieves.

3. Instrumental details

Powder X-ray diffraction (PXRD):

Powder X-ray diffraction (PXRD) for all the MOF samples were collected on a PANalytical Empyrean diffractometer in Bragg-Brentano geometry using Cu-Kα radiation (λ = 1.54187 Å), operational at 45 kV and 40 mA. The incident beam was equipped with a Bragg-Brentano HD X-ray optic using fixed slits/soller slits. The detector was a silicon-based linear position sensitive X'Celerator Scientific operating in 1-D scanning mode. Data were collected from 5 to 50° 2θ using a step size of 0.0083° and a count time of at least 10 s per step. Powder patterns were processed using Data Viewer PANalytical and OriginPro 8 software.

Gas sorption measurements:

Sorption experiments were carried out using a NOVA e series 4200 surface area analyzer (Quantachrome Instruments, Boynton Beach, Florida, USA). N_2 (99.999%) was purchased from Cryogenic Gases and used as received. For N_2 measurements, a glass sample cell was charged with ~30 mg sample and analyzed at 77 K. Sorption isotherms were collected in the NOVAwin software.

^{1}H-NMR measurement:

All ^{1}H-NMR measurements were carried out on a Varian MR400 (400 MHz (9.4 Tesla) spectrometer.

4. MOF synthesis and activation procedure

4.1. Synthesis of DUT-23-Cu and activation:

The synthesis was based on a published literature procedure with slight modifications.[21] $Cu(NO_3)_2 \cdot 2.5H_2O$ (241.0 mg, 1.036 mmol), bipyridine (42.20 mg, 0.2702 mmol), and 1,3,5-tris(4-carboxyphenyl)benzene (109.0 mg, 0.2486 mmol) were dissolved in a mixture of DMF (5 mL), EtOH (abs., 5 mL), and 50 µl of trifluoroacetic acid. The mixture was sonicated for 5 min and heated at 80 °C for 20 h in a screw-capped vial (20 mL). Light-blue clear crystals of a

single phase were obtained. Crystals of DUT-23-Cu were washed with fresh DMF two times and then exchanged with ethanol. Ethanol exchange was performed for four days, with two exchanges each day. Ethanol solvated crystals were then activated by flowing liquid CO_2 at 2 mL/min flowrate for 2 h at room temperature, subsequently by supercritical CO_2 at a flow rate of 2 mL/min for 3 h at 55 °C and finally by supercritical CO_2 at a flow rate of 1 mL/min for 3 h at 55 °C.[22]

4.2. Synthesis of UMCM-152 and activation:

Ligand synthesis for UMCM-152:

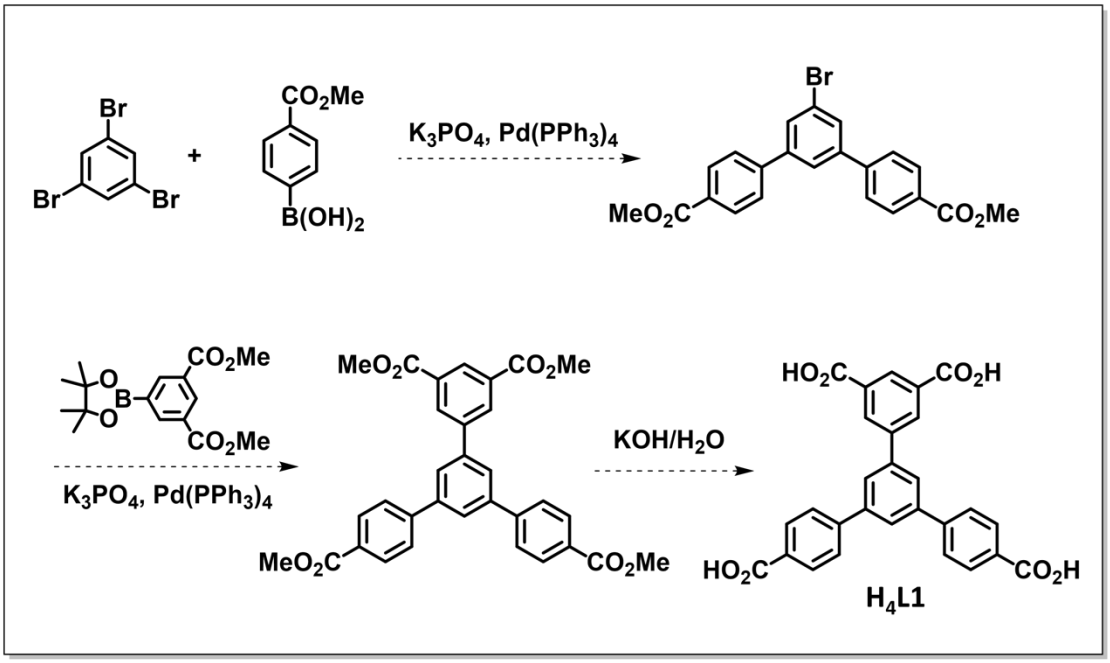

Scheme S1. Synthesis of the organic linker (H4L1) for UMCM-152.

UMCM-152 was synthesized following a reported literature procedure with slight modifications.[19] The linker 5'-(4 carboxyphenyl)-[1,1':3',1"-terphenyl] 3,4",5-tricarboxylic acid (**H_4L1**) (50.05 mg, 0.1036 mmol) was added to a solution of 0.005 M HCl in DMF/dioxane/H_2O (4:1:1, 10 ml). To this mixture, $Cu(NO_3)_2 \cdot 2.5H_2O$ (96.04 mg, 0.4129 mmol) was added, and the contents were sonicated until dissolved and then heated at 85 ºC for about 18 h in a screw-capped vial (20 mL). Blue block crystals were obtained which were washed repeatedly with DMF to ensure that it is free from unreacted linker. The MOF was exchanged with dry MeOH for three consecutive days, four times wash each day. The sample was further treated with dry acetone. After removing acetone by decanting, the sample was dried under vacuum (0.03 Torr) at room temperature (4 h), and then further heated at 100 ºC for 20 h leading to a color change from sky blue to dark purple.

4.3. Synthesis of UTSA-76 and activation:

Ligand synthesis for UTSA-76:

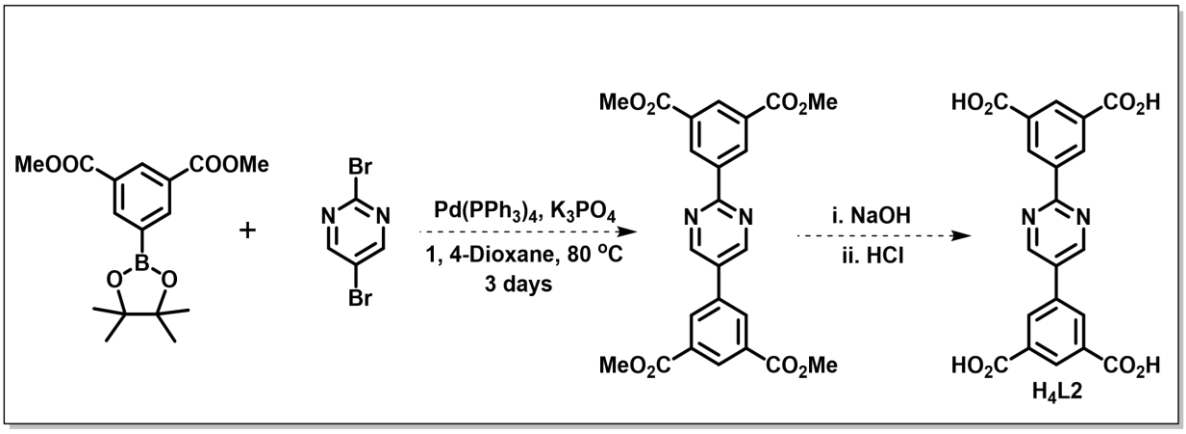

Scheme S2. Synthesis of the organic linker (H4L2) for UTSA-76.

The linker for UTSA-76 was synthesized following literature procedure with some modifications.[20] $Cu(NO_3)_2 \cdot 2.5H_2O$ (80.2 mg, 0.344 mmol) and the organic linker, 5,5'-(pyrimidine-2,5-diyl) diisophthalic acid (**H_4L2**) (30.5 mg, 0.0742 mmol) were dissolved into mixed solvents (DMF/MeCN/H_2O, 6/1/1, v/v) of 8 mL, in a screw-capped vial (20 mL). Subsequently, 50 µL of 37% HCl was added to this mixture solution. The vial was capped, sonicated for ~5 minutes and heated in an oven at 85 ˚C for 24 h. Blue block crystals were formed at the bottom of the vial, which were obtained by filtration and washed several times with DMF to afford UTSA-76. Subsequently, crystals of UTSA-76 were exchanged with ethanol and immersed for three days. The supernatant liquid was replaced with fresh ethanol two times (20 mL × 2) each day. The MOF was then activated by flowing supercritical CO_2 for a period of 5 h. Following supercritical activation, the crystals were further heated under dynamic vacuum (0.01 Torr) at 80 ˚C for 12 h and then again at 110 ˚C for another 5 h to afford purple crystalline material.

5. Characterization of linkers and intermediates by NMR spectroscopy

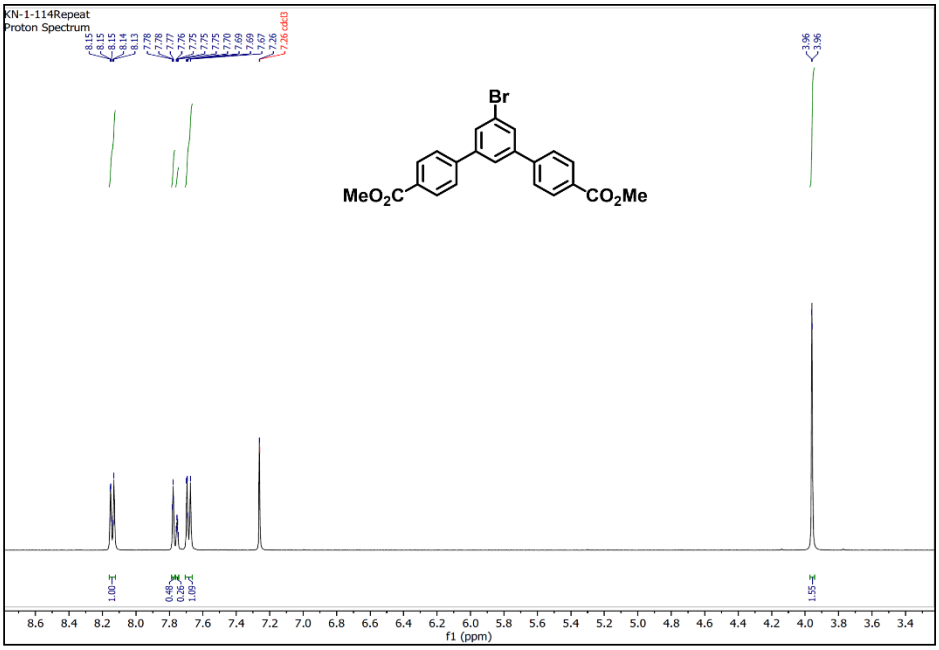

Figure S1. ^{1}H NMR (400 MHz) spectra of dimethyl 5'-bromo-[1,1':3',1''-terphenyl]-4,4''-dicarboxylate in $CDCl_3$.

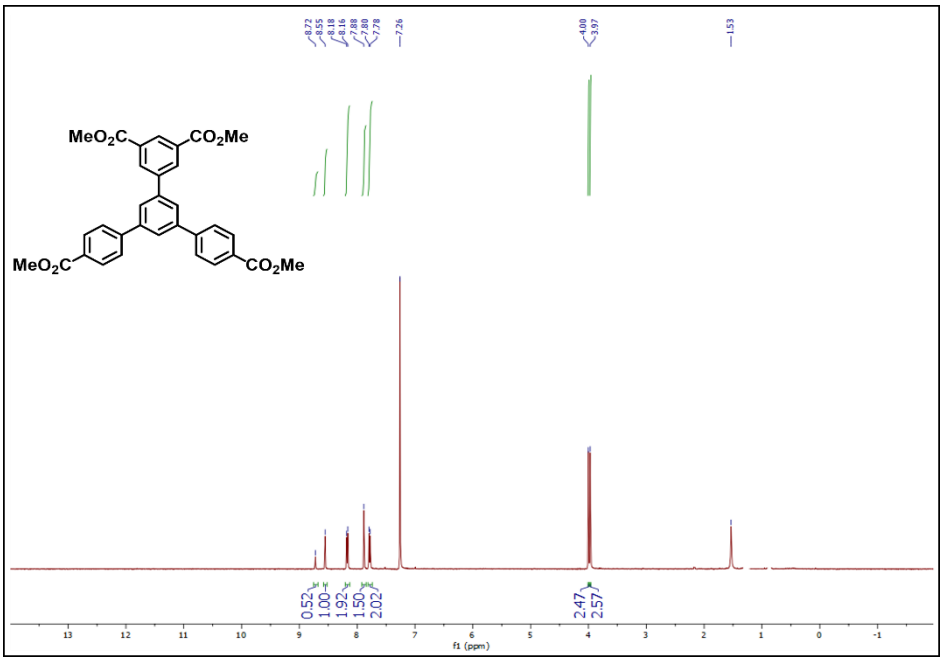

Figure S2. ^{1}H NMR (400 MHz) spectra of trimethyl 5'-(4-(methoxycarbonyl)phenyl)-[1,1':3',1''-terphenyl]-3,4'',5-tricarboxylate in $CDCl_3$.

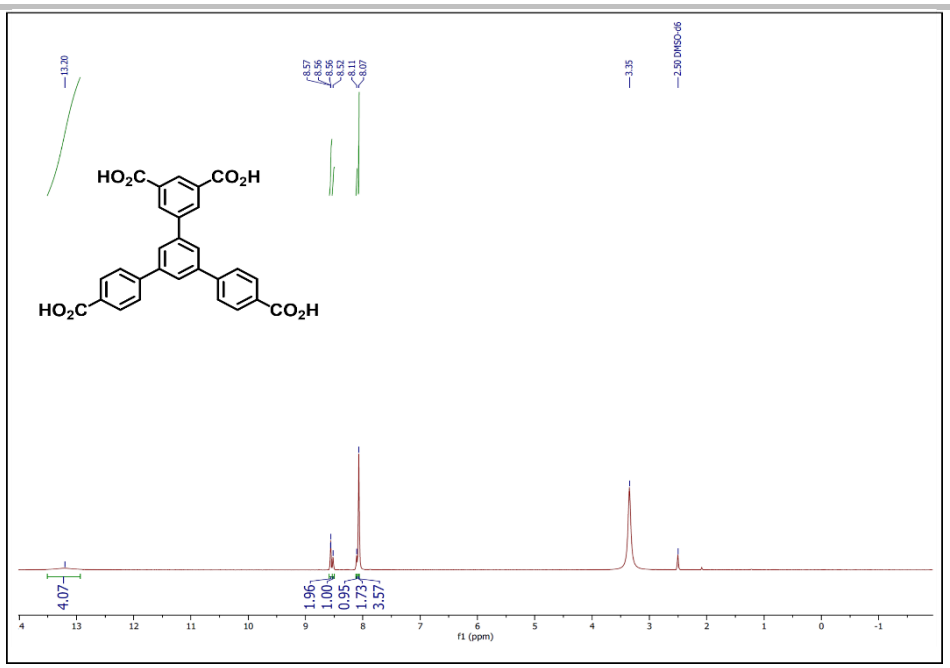

Figure S3. ^{1}H NMR (400 MHz) spectra of 5'-(4-carboxyphenyl)-[1,1':3',1''-terphenyl]-3,4'',5-tricarboxylic acid in DMSO-d_6.

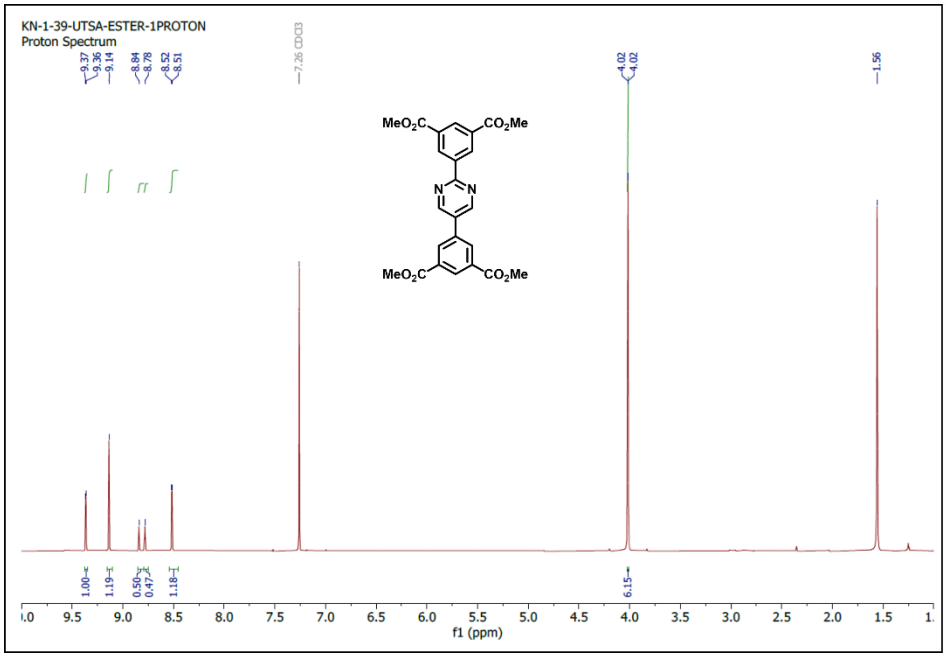

Figure S4. ^{1}H NMR (400 MHz) spectra of tetramethyl 5,5'-(pyrimidine-2,5-diyl)diisophthalate in $CDCl_3$.

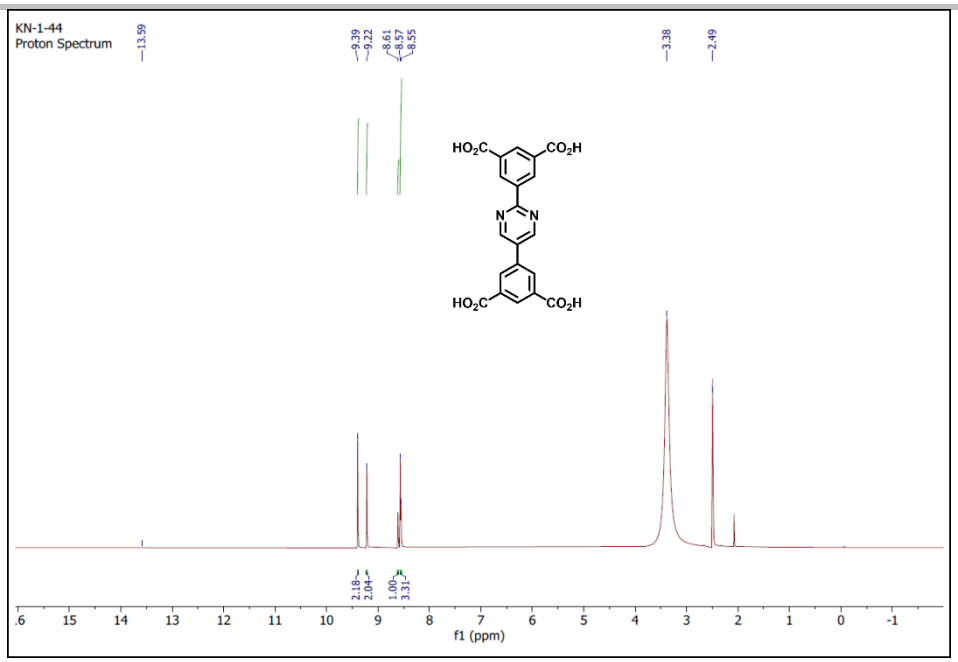

Figure S5. ^{1}H NMR (400 MHz) spectra of 5,5'-(pyrimidine-2,5-diyl)diisophthalic acid in DMSO-d_6.

6. Powder X-ray diffraction patterns

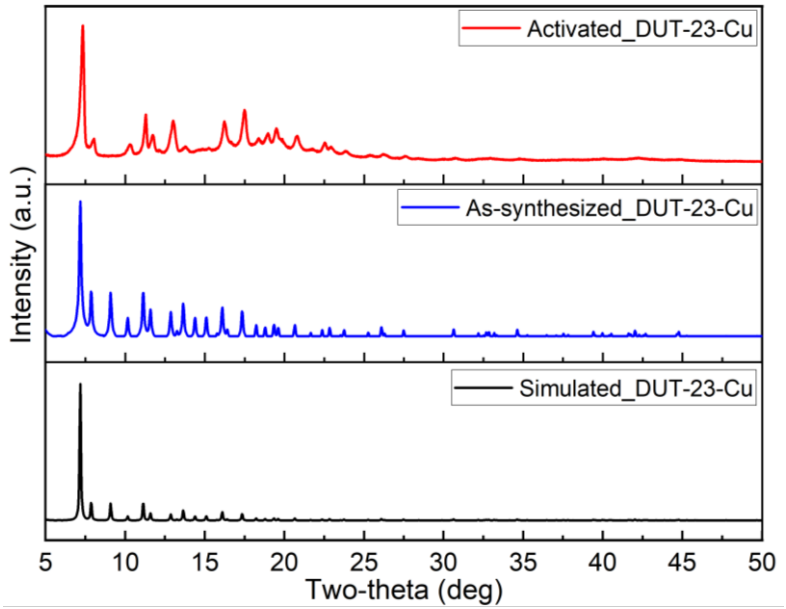

Figure S6. Comparison of simulated (black), as-synthesized (blue) and activated (red) powder X-ray diffraction patterns of DUT-23-Cu.

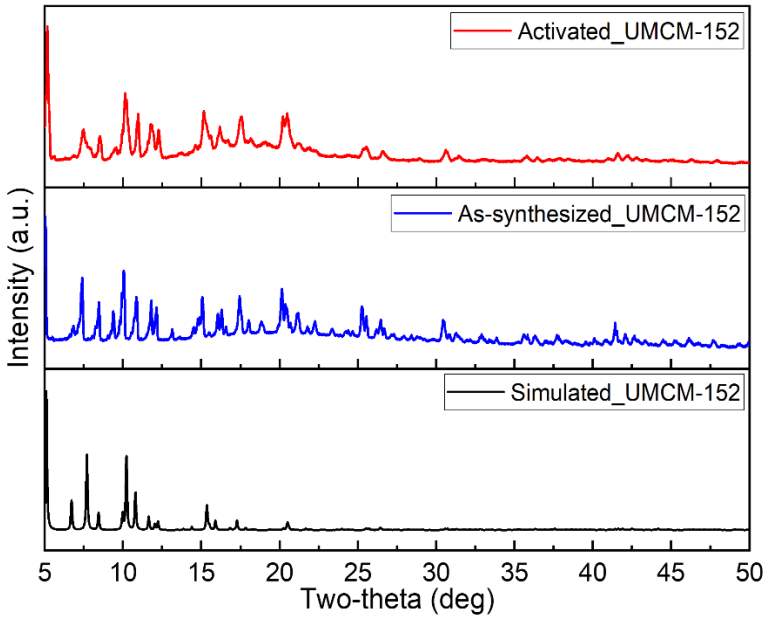

Figure S7. Comparison of simulated (black), as-synthesized (blue) and activated (red) powder X-ray diffraction patterns of UMCM-152.

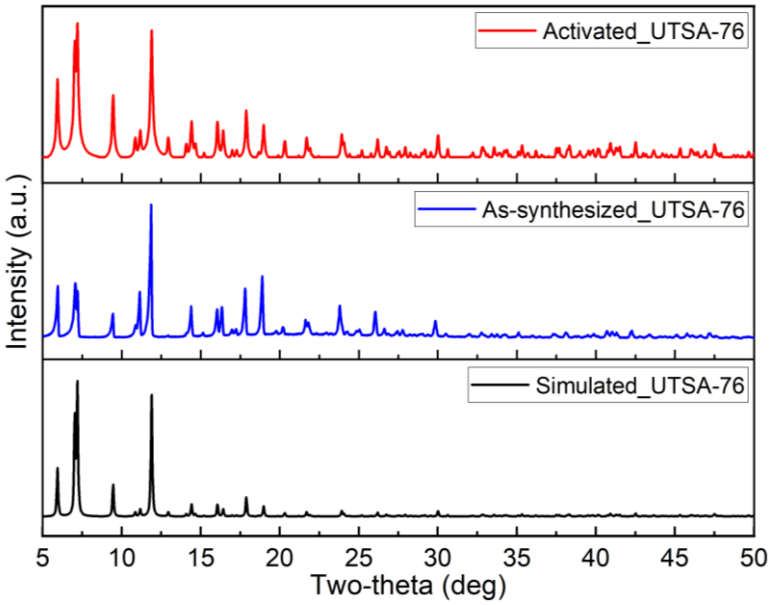

Figure S8. Comparison of simulated (black), as-synthesized (blue) and activated (red) powder X-ray diffraction patterns of UTSA-76.

7. Measured nitrogen adsorption isotherms

BET surface area = 2700.405 ± 18.524 m^2/g

C constant = 4234.706

Correlation coefficient, r = 0.999998

BET fitting range = [0.001, 0.0287]

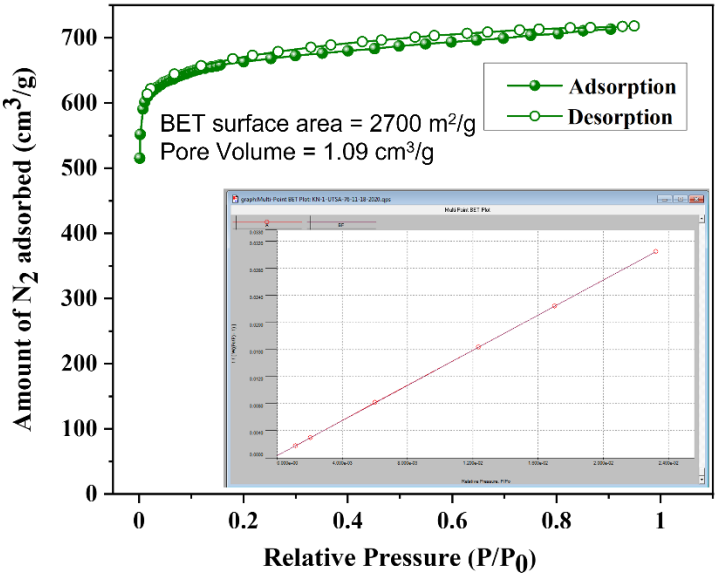

Figure S9. Nitrogen adsorption-desorption isotherm at 77 K for activated UTSA-76, with BET surface area determined within the fitting range (P/P_0 = 0.001-0.0287).

BET surface area = 3430.583 ± 30.432 m^2/g

C constant = 1267.149

Correlation coefficient, r = 0.999991

BET fitting range = [0.022, 0.053]

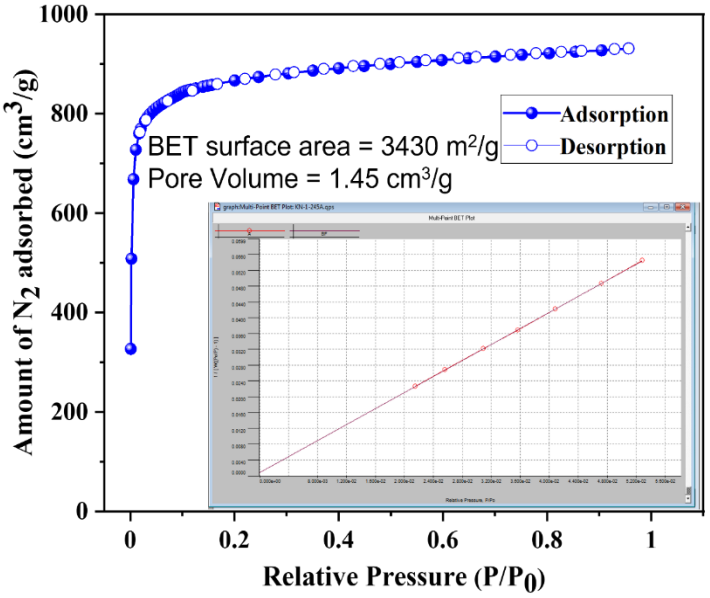

Figure S10. Nitrogen adsorption-desorption isotherm at 77 K for activated UMCM-152, with BET surface area determined within the fitting range (P/P_0 = 0.022-0.053).

BET surface area = 5300.090 ± 25.634 m^2/g

C constant = 149.164

Correlation coefficient, r = 0.999913

BET fitting range = [0.051, 0.080]

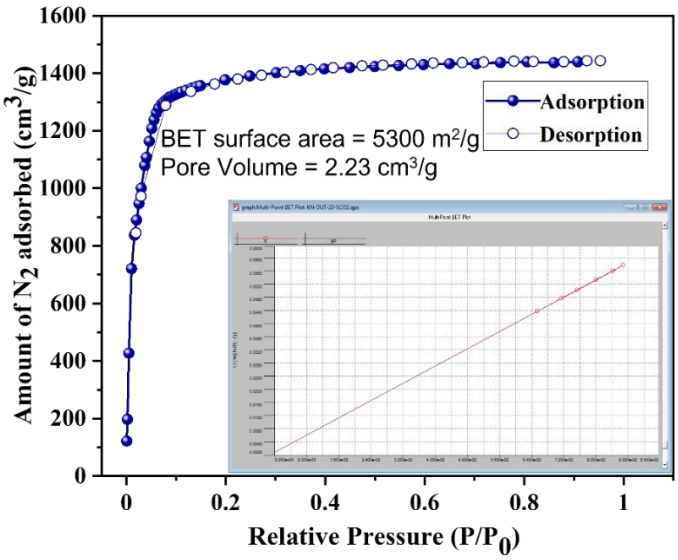

Figure S11. Nitrogen adsorption-desorption isotherm at 77 K for activated DUT-23-Cu, with BET surface area determined within the fitting range (P/P_0 = 0.051-0.080).

8. High pressure CH_4 adsorption measurements

High-pressure methane adsorption isotherms were measured on a fully automated Sievert's-type instrument PCT-Pro from SETARAM. Ultra-high purity grade CH_4 and He (99.999% purity) gases were used for the high-pressure adsorption experiments. Activated MOF samples were loaded into a stainless-steel sample holder inside a high-purity nitrogen glove box. The sample holder was then connected to the instrument's analysis station *via* VCR fittings using a ½ inch fritted copper gasket (2 micron) and evacuated at room temperature for about an hour.

The sample holder was immersed into a recirculating bath, that was connected to a temperature controlled programmable isothermal bath filled with a solution of ethylene glycol-H_2O and the sample temperature was maintained at 25.3 ºC. Helium was used to perform void volume measurements by the method of expansion from a known reservoir volume to the sample cell and then recording the change in the pressure, assuming negligible He adsorption. Generally, two volume calibrations were performed, one to determine the apparent volume at instrument temperature (V_{so}) and the other to determine the apparent volume at the experimental/sample temperature (V_{sa}).

Excess adsorption and desorption amounts were determined by the PCT-Pro software using a mass balance analysis as a function of the equilibrium pressure. The excess adsorption isotherms were further corrected using background adsorption corrections, measured with an empty sample holder under similar experimental conditions. Total volumetric methane capacities were then determined using the following equation.[23,24]

$$n_{total} = n_{excess} + V_p \cdot \rho_{bulk}\ (T, P)$$

where, n_{total} represents total volumetric adsorption capacity,

n_{excess} represents the experimentally measured excess adsorption,

V_p indicates the total pore volume as determined (at P/P_0 = 0.95) from N_2 adsorption experiment at 77K and ρ_{bulk} indicates the bulk density of methane at specific pressures (298 K) obtained from NIST REFPROF database.[25]

9. Comparison between experimental and calculated adsorption isotherms

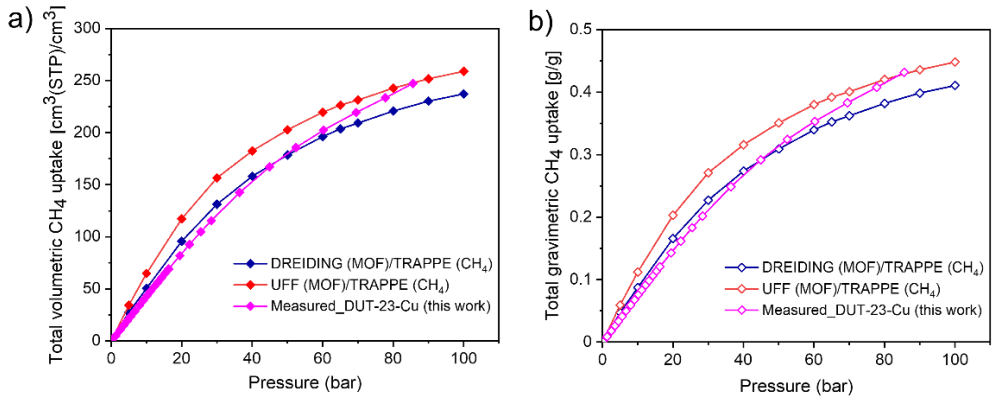

Figure S12. Measured and calculated (a) total volumetric and (b) total gravimetric methane adsorption isotherms for DUT-23-Cu at 298 K. Calculated isotherms are shown for two choices of the interatomic potentials: DREIDING (MOF) / TRAPPE (CH_4) and UFF (MOF) / TRAPPE (CH_4).

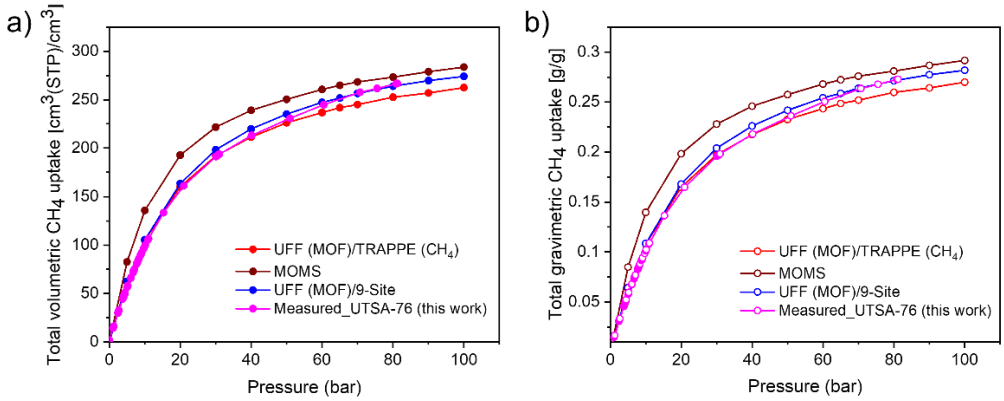

Figure S13. Measured and calculated (a) total volumetric and (b) total gravimetric methane adsorption isotherms for UTSA-76 at 298 K. Calculated isotherms are shown for 3 choices of the interatomic potentials: UFF (MOF) / TRAPPE (CH_4), MOMS, and UFF (MOF) / 9-site (CH_4).

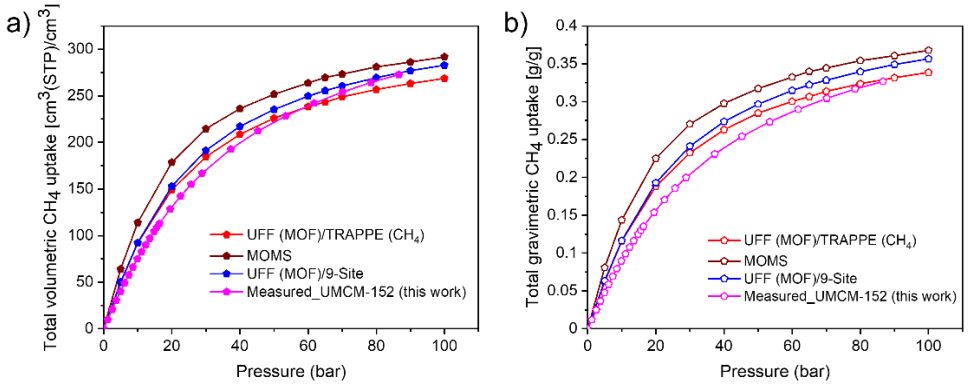

Figure S14. Measured and calculated (a) total volumetric and (b) total gravimetric methane adsorption isotherms for UMCM-152 at 298 K. Calculated isotherms are shown for 3 choices of the interatomic potentials: UFF (MOF) / TRAPPE (CH_4), MOMS, and UFF (MOF) / 9-site (CH_4).

10. Experimental volumetric and gravimetric methane isotherms

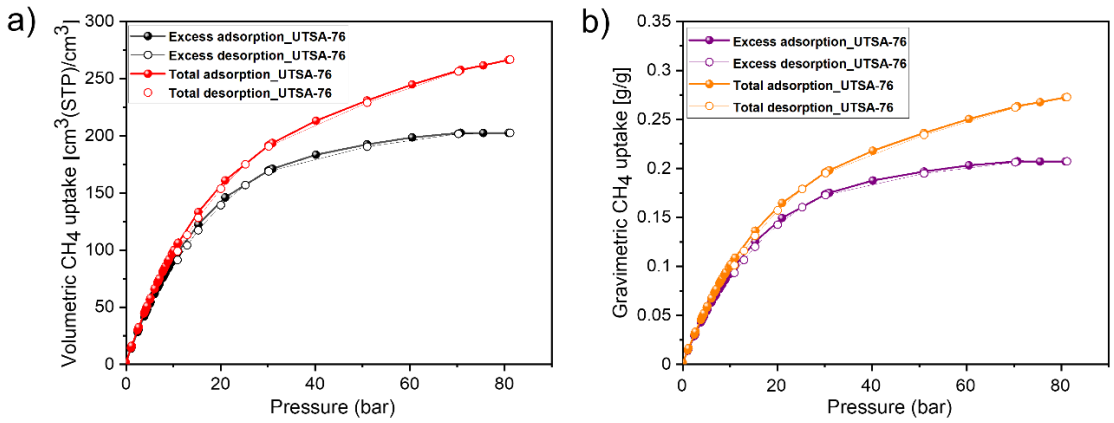

Figure S15. Measured (a) volumetric and (b) gravimetric methane uptake in UTSA-76 at 298 K.

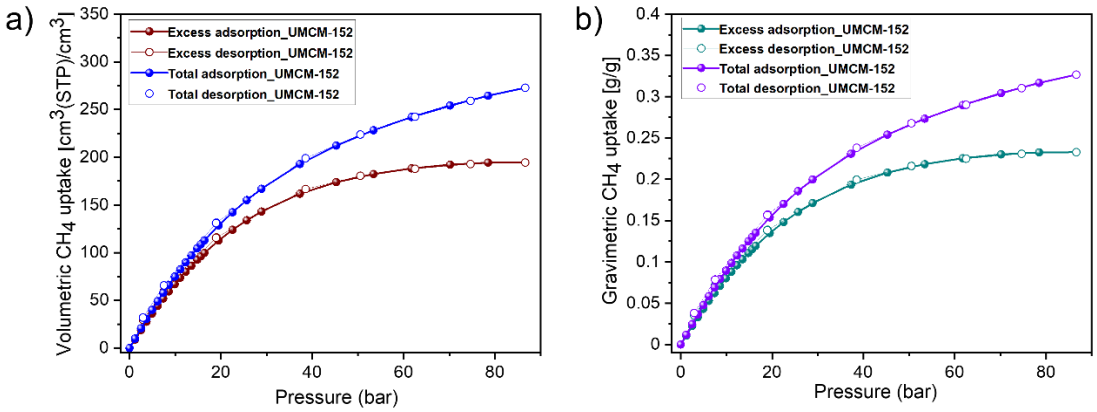

Figure S16. Measured (a) volumetric and (b) gravimetric methane uptake in UMCM-152 at 298 K.

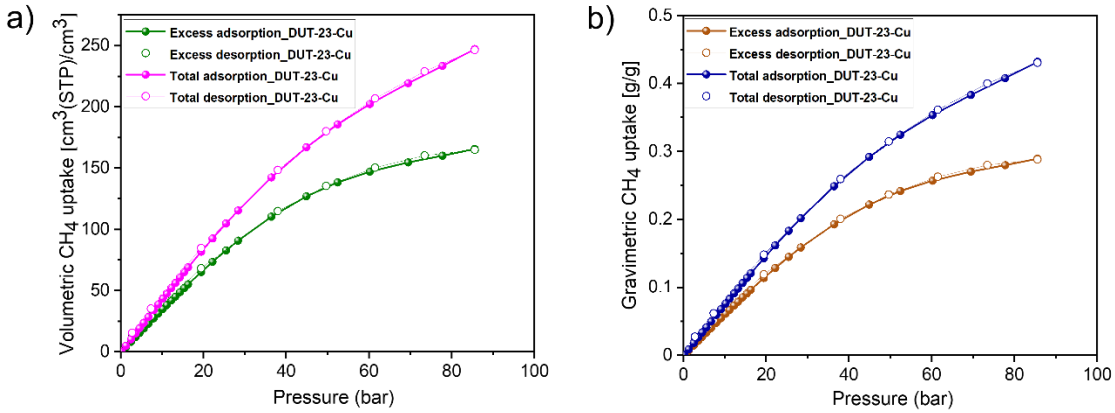

Figure S17. Measured (a) volumetric and (b) gravimetric methane uptake in DUT-23-Cu at 298 K.

11. Test on repeatability and recyclability

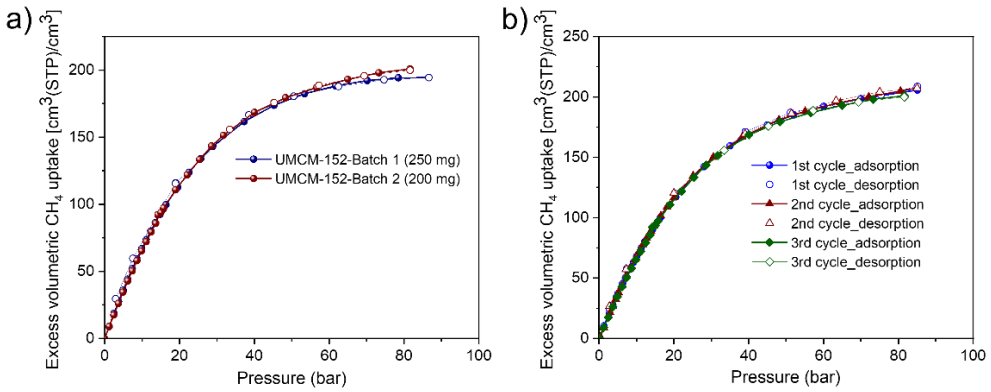

Figure S18. (a) Excess volumetric methane uptake, measured at 298 K, from two different UMCM-152 sample batches, where MOFs prepared under same procedure. (b) Cyclic adsorption and desorption measurements on UMCM-152 (Batch 1) at 298 K with approx. ± 2.3% errors in the high-pressure region.

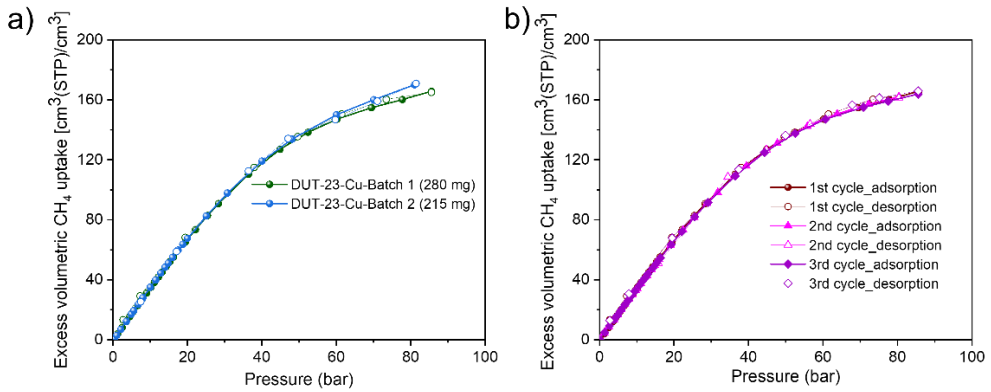

Figure S19. (a) Excess volumetric methane uptake, measured at 298 K, from two different DUT-23-Cu sample batches, where MOFs prepared under same procedure. (b) Cyclic adsorption and desorption measurements on DUT-23-Cu (Batch 1) at 298 K with approx. ± 1.0% errors in the high-pressure region.

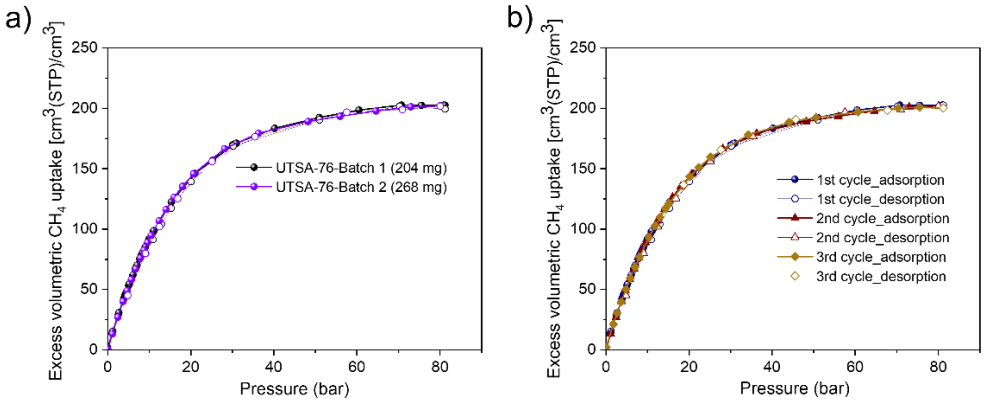

Figure S20. (a) Excess volumetric methane uptake, measured at 298 K, from two different UTSA-76 sample batches, where MOFs prepared under same procedure. (b) Cyclic adsorption and desorption measurements on UTSA-76 (Batch 1) at 298 K with approx. ± 0.9% errors in the high-pressure region.

Table S6. Comparison of experimentally determined volumetric deliverable capacities of the best MOFs at 298 K.

MOFs	BET surface area (m^2/g)	Pore volume (cm^3/g)	Crystal density (g/cm^3)	Total CH_4 uptake at 65 bar (cm^3@STP /cm^3)	Deliverable capacity (5 to 65 bar) (cm^3@STP/cm^3)	Total CH_4 uptake at 80 bar (cm^3@STP /cm^3)	Deliverable capacity (5 to 80 bar) (cm^3@STP/cm^3)	References
MFM-115a	3394	1.38	0.611	238	191	256	208	26
MOF-905	3490	1.34	0.537	206	181	228	203	27
Al-soc-MOF-1	5585	2.3	0.34	197	176	221	201	28
HKUST-1	1850	0.78	0.883	267	190	272	200	24, 29
UTSA-76a	2820	1.09	0.699	257	196	-	-	20
UTSA-76a	2700	1.09	0.699	251	195	266	210	**This work**
UMCM-152	3430	1.45	0.598	247	207	266	226	**This work**
DUT-23-Cu	5300	2.23	0.41	211	190	237	216	**This work**
MOF-519	2400	0.938	0.953	260	209	279	230	30
MOF-520	3290	1.277	0.586	217	180	231	194	30
PCN-14	2000	0.85	0.829	230	157	250	178	24, 29, 31
MOF-177	4500	1.89	0.427	193	175	205	185	32
NJU-BAI-43	3090	1.22	0.639	254	198	-	-	33
Co(bdp)	2911	1.02	0.774	203	197	-	-	34
MAF-38	2022	0.808	0.76	263	187	273	197	35
MFU-4l-Li[a]	4070	1.66	0.479	205	177	226	198	36
NU-1501-Al[a]	7310	2.91	0.283	163	147	190	174	37
NU-1501-Fe[a]	7140	2.90	0.299	168	151	193	176	37
ST-2	5172	2.44	0.366	181	160	206	185	38

[a] Data collected at 296 K.

SUPPORTING INFORMATION

References

[1] T. F. Willems, C. H. Rycroft, M. Kazi, J. C. Meza, M. Haranczyk, *Microporous Mesoporous Mater*. **2012**, *149* (1), 134–141.
[2] M. Pinheiro, R. L. Martin, C. H. Rycroft, M. Haranczyk, *CrystEngComm* **2013**, *15* (37), 7531–7538.
[3] M. Haranczyk, R. L. Martin, Mathematical Tools for Discovery of Nanoporous Materials for Energy Applications. *J. Phys. Conf. Ser* **574**.
[4] A. K. Rappe, C. J. Casewit, K. S. Colwell, W. A. Goddard, W. M. Skiff, *J. Am. Chem. Soc.* **1992**, *114* (25), 10024–10035.
[5] M. G. Martin, J. I. Siepmann, *J. Phys. Chem. B* **1998**, *102* (14), 2569–2577.
[6] S. L. Mayo, B. D. Olafson, W. A. Goddard III, *J. Phys. Chem* **1990**, *94* (91), 8897–8909.
[7] C. R. Cioce, Computational Investigations of Potential Energy Function Development for Metal-Organic Framework Simulations, Metal Carbenes, and Chemical Warfare Agents, University of South Florida, **2015**.
[8] C. R. Cioce, K. McLaughlin, J. L. Belof, B. Space, *J. Chem. Theory Comput*. **2013**, *9* (12), 5550–5557.
[9] H. S. Koh, M. K. Rana, A. G. Wong-Foy, D. J. Siegel, *J. Phys. Chem. C* **2015**, *119* (24), 13451–13458.
[10] R. J. Sadus, Molecular Simulation of Fluids: Theory, Algorithms, and Object-Orientation.; Elsevier: Amsterdam, **1999**.
[11] D. Frenkel, B. Smit, Understanding Molecular Simulation : From Algorithms to Applications, 2nd ed.; Academic Press, Inc.: Orlando, FL, **2001**.
[12] D. Dubbeldam, A. Torres-Knoop, K. S. Walton, *Mol. Simul.* **2013**, *39*, 14–15.
[13] S. I. Sandler, An Introduction to Applied Statistical Thermodynamics; John Wiley & Son Ltd: New York, NY, **2010**.
[14] T. L. Hill, An Introduction to Statistical Thermodynamics; Dover Publications, **1986**.
[15] D. Dubbeldam, S. Calero, D. E. Ellis, R. Q, Snurr, *Mol. Simul.* **2016**, *42* (2), 81–101.
[16] A. K. Rappe, W. A. Goddard III, *J. Phys. Chem*. **2002**, *95* (8), 3358–3363.
[17] D. Ongari, P. G. Boyd, O. Kadioglu, A. K. Mace, S. Keskin, B. Smit, *J. Chem. Theory Comput*. **2019**, *15* (1), 382–401.
[18] Y. G. Chung, E. Haldoupis, B. J. Bucior, M. Haranczyk, S. Lee, H. Zhang, K. D. Vogiatzis, M. Milisavljevic, S. Ling, J. S. Camp, B. Slater, J. I. Siepmann, D. S. Sholl, R. Q. Snurr, *J. Chem. Eng. Data* **2019**, *64* (12), 5985–5998.
[19] J. K. Schnobrich, O. Lebel, K. A. Cychosz, A. Dailly, A. G. Wong-Foy, A. J. Matzger, *J. Am. Chem. Soc*. **2010**, *132*, 13941−13948.
[20] B. Li, H.-M.Wen, H. Wang, H. Wu, M. Tyagi, T. Yildirim, W. Zhou, B. Chen, *J. Am. Chem. Soc*. **2014**, *136*, 6207–6210.
[21] N. Klein, I. Senkovska, I. A. Baburin, R. Gruenker, U. Stoeck, M. Schlichtenmayer, B. Streppel, U. Mueller, S. Leoni, M. Hirscher, S. Kaskel, *Chem. Eur. J*. **2011**, *17*, 13007−13016.
[22] B. Liu, A. G. Wong-Foy, A. J. Matzger, *Chem. Commun*. **2013**, *49* (14), 1419−1421.
[23] W. Zhou, H. Wu, M. R. Hartman, T. Yildirim, *J. Phys. Chem. C* **2007**, *111*, 16131−16137.
[24] J. A. Mason, M. Veenstra, J. R. Long, *Chem. Sci.* **2014**, *5*, 32–51.
[25] (a) E. W. Lemmon, M. L. Huber and M. O. McLinden, NIST Standard Reference Database 23: Reference Fluid Thermodynamic and Transport Properties-REFPROP, Version 8.0, National Institute of Standards and Technology, Standard Reference Data Program, Gaithersburg, **2007**.
(b) U. Setzmann and W. Wagner, *J. Phys. Chem. Ref. Data*, **1991**, *20*, 1061.
[26] Y. Yan, D. I. Kolokolov, I. da Silva, A. G. Stepanov, A. J. Blake, A. Dailly, P. Manuel, C. C. Tang, S. Yang, M. Schroder, *J. Am. Chem. Soc*. **2017**, *139*, 13349–13360.
[27] J. Jiang, H. Furukawa, Y.-B. Zhang, O. M. Yaghi, *J. Am. Chem. Soc*. **2016**, *138*, 10244−10251.
[28] D. Alezi, Y. Belmabkhout, M. Suyetin, P. M. Bhatt, L. J. Weselinski, V. Solovyeva, K. Adil, I. Spanopoulos, P. N. Trikalitis, A.-H. Emwas, M. Eddaoudi, *J. Am. Chem. Soc*. **2015**, *137*, 13308−13318.
[29] Y. Peng, V. Krungleviciute, I. Eryazici, J. T. Hupp, O. K. Farha, T. Yildirim, *J. Am. Chem. Soc*. **2013**, *135*, 11887−11894.
[30] F. Gándara, H. Furukawa, S. Lee, O. M. Yaghi, *J. Am. Chem. Soc*. **2014**, *136*, 5271−5274.
[31] S. Ma, D. Sun, J. M. Simmons, C. D. Collier, D. Yuan, H.-C. Zhou, *J. Am. Chem. Soc*. **2008**, *130*, 1012−1016.
[32] H. Furukawa, N. Ko, Y. B. Go, N. Aratani, S. B. Choi, E. Choi, A. Ö. Yazaydin, R. Q. Snurr, M. O'Keeffe, J. Kim, O. M. Yaghi, *Science* **2010**, *329*, 424–428.
[33] M. Zhang, W. Zhou, T. Pham, K. A. Forrest, W. Liu, Y. He, H. Wu, T. Yildirim, B. Chen, B. Space, Y. Pan, M. J. Zaworotko, J. Bai, *Angew. Chem. Int. Ed*. **2017**, *56*, 11426−11430.
[34] J. A. Mason, J. Oktawiec, M. K. Taylor, M. R. Hudson, J. Rodriguez, J. E. Bachman, M. I. Gonzalez, A. Cervellino, A. Guagliardi, C. M. Brown, P. L. Llewellyn, N. Masciocchi, J. R. Long, *Nature* **2015**, *527*, 357–361.
[35] J.-M. Lin, C.-T. He, Y. Liu, P.-Q. Liao, D.-D. Zhou, J.-P. Zhang, X.-M. Chen, *Angew. Chem*. **2016**, *128*, 4752–4756.
[36] Z. Chen, M. R. Mian, S.-J. Lee, H. Chen, X. Zhang, K. O. Kirlikovali, S. Shulda, P. Melix, A. S. Rosen, P. A. Parilla, T. Genett, R. Q. Snurr, T. Islamoglu, T. Yildirim, O. K. Farha, *J. Am. Chem. Soc.* **2021**, *143*, 18838–18843.
[37] Z. Chen, P. Li, R. Anderson, X. Wang, X. Zhang, L. Robison, L. R. Redfern, S. Moribe, T. Islamoglu, D. A. Gómez-Gualdrón, T. Yildirim, J. F. Stoddart, O. K. Farha, *Science* **2020**, *368*, 297–303.
[38] C.-C. Liang, Z.-L. Shi, C.-T. He, J. Tan, H.-D. Zhou, H.-L. Zhou, Y. Lee, Y.-B. Zhang, *J. Am. Chem. Soc*. **2017**, *139*, 13300–13303.